ISSN 1674-1056
http://cpb.iphy.ac.cn
http://iopscience.iop.org/cpb
中国物理 B
Chinese Physics
中国物理 Chinese Physics B

A review on MBE-grown HgCdSe infrared materials on GaSb (211)B substrates

Z K Zhang, W W Pan, J L Liu, W Lei

Citation: Chin. Phys. B . 2019, 28(1): 018103. **doi:** 10.1088/1674-1056/28/1/018103
Journal homepage: http://cpb.iphy.ac.cn; http://iopscience.iop.org/cpb

What follows is a list of articles you may be interested in

1.3-μm InAs/GaAs quantum dots grown on Si substrates

Fu-Hui Shao(邵福会), Yi Zhang(张一), Xiang-Bin Su(苏向斌), Sheng-Wen Xie(谢圣文), Jin-Ming Shang(尚金铭), Yun-Hao Zhao(赵云昊), Chen-Yuan Cai(蔡晨元), Ren-Chao Che(车仁超), Ying-Qiang Xu(徐应强), Hai-Qiao Ni(倪海桥), Zhi-Chuan Niu(牛智川)

Chin. Phys. B . 2018, 27(12): 128105. **doi:** 10.1088/1674-1056/27/12/128105

Growth of high-quality perovskite (110)-$SrIrO_3$ thin films using reactive molecular beam epitaxy

Kai-Li Zhang(张凯莉), Cong-Cong Fan(樊聪聪), Wan-Ling Liu(刘万领), Yu-Feng Wu(吴宇峰), Xiang-Le Lu(卢祥乐), Zheng-Tai Liu(刘正太), Ji-Shan Liu(刘吉山), Zhong-Hao Liu(刘中灏), Da-Wei Shen(沈大伟)

Chin. Phys. B . 2018, 27(8): 088103. **doi:** 10.1088/1674-1056/27/8/088103

Effects of growth conditions on optical quality and surface morphology of InGaAsBi

Jia-Kai Li(李家恺), Li-Kun Ai(艾立鹍), Ming Qi(齐鸣), An-Hui Xu(徐安怀), Shu-Min Wang(王庶民)

Chin. Phys. B . 2018, 27(4): 048101. **doi:** 10.1088/1674-1056/27/4/048101

Nucleation of GaSb on GaAs (001) by low pressure metal-organic chemical vapor deposition

Wang Lian-Kai, Liu Ren-Jun, Yang Hao-Yu, Lü You, Li Guo-Xing, Zhang Yuan-Tao, Zhang Bao-Lin

Chin. Phys. B . 2014, 23(8): 088110. **doi:** 10.1088/1674-1056/23/8/088110

Improved interfacial and electrical properties of GaSb metal oxide semiconductor devices passivated with acidic $(NH_4)_2S$ solution

Zhao Lian-Feng, Tan Zhen, Wang Jing, Xu Jun

Chin. Phys. B . 2014, 23(7): 078102. **doi:** 10.1088/1674-1056/23/7/078102

TOPICAL REVIEW — Photodetector: Materials, physics, and applications

A review on MBE-grown HgCdSe infrared materials on GaSb (211)B substrates*

Z K Zhang, W W Pan, J L Liu, and W Lei†

Department of Electrical, Electronic and Computer Engineering, The University of Western Australia, 35 Stirling Highway, Crawley 6009, Australia

(Received 23 October 2018; published online 25 December 2018)

We review our recent efforts on developing HgCdSe infrared materials on GaSb substrates via molecular beam epitaxy (MBE) for fabricating next generation infrared detectors with features of lower production cost and larger focal plane array format size. In order to achieve high-quality HgCdSe epilayers, ZnTe buffer layers are grown before growing HgCdSe, and the study of misfit strain in ZnTe buffer layers shows that the thickness of ZnTe buffer layer needs to be below 300 nm in order to minimize the generation of misfit dislocations. The cut-off wavelength/alloy composition of HgCdSe materials can be varied in a wide range by varying the ratio of Se/Cd beam equivalent pressure during the HgCdSe growth. Growth temperature presents significant impact on the material quality of HgCdSe, and lower growth temperature leads to higher material quality for HgCdSe. Typically, long-wave infrared HgCdSe ($x = 0.18$, cut-off wavelength of 10.4 μm at 80 K) presents an electron mobility as high as 1.3×10^5 cm$^2\cdot$V$^{-1}\cdot$s^{-1}, a background electron concentration as low as 1.6×10^{16} cm^{-3}, and a minority carrier lifetime as long as 2.2 μs. These values of electron mobility and minority carrier lifetime represent a significant improvement on previous studies of MBE-grown HgCdSe reported in the open literatures, and are comparable to those of counterpart HgCdTe materials grown on lattice-matched CdZnTe substrates. These results indicate that HgCdSe grown at the University of Western Australia, especially long-wave infrared can meet the basic material quality requirements for making high performance infrared detectors although further effort is required to control the background electron concentration to below 10^{15} cm^{-3}. More importantly, even higher quality HgCdSe materials on GaSb are expected by further optimizing the growth conditions, using higher purity Se source material, and implementing post-growth thermal annealing and defect/impurity gettering/filtering. Our results demonstrate the great potential of HgCdSe infrared materials grown on GaSb substrates for fabricating next generation infrared detectors with features of lower cost and larger array format size.

Keywords: infrared detector, HgCdSe, GaSb, molecular beam epitaxy

PACS: 81.05.Dz, 61.72.uj, 73.61.Ga **DOI:** 10.1088/1674-1056/28/1/018103

1. Introduction

1.1. Infrared detectors

The infrared band is a portion of electromagnetic spectrum, the wavelength of which ranges from 0.7 μm to 1 mm. This portion of electromagnetic spectrum is very special because it covers the main transmission windows of atmosphere. Figure 1 shows the typical transmission spectrum of atmosphere.[1] It is observed that generally the atmosphere presents strong absorption of some molecules mainly H_2O and CO_2. However, there are several high transmission windows in the infrared band region, which can be utilized for communication, imaging, and remote sensing through the atmosphere. According to the high transmission windows in the atmosphere, infrared band can be further divided into four main sub-bands, namely, short-wave infrared (SWIR, 1–3 μm), mid-wave infrared (MWIR, 3–5 μm), long-wave infrared (LWIR, 8–12 μm), and very-long-wave infrared (VLWIR, above 12 μm). Because many objects present thermal radiation in these wavelength ranges, these infrared sub-bands (SWIR, MWIR, LWIR, and VLWIR) can be used to identify objects, and thus have a wide range of applications in various industry areas such as remote sensing, night vision, astronomy study, chemical analysis, and so on. For infrared applications, the most critical electronic component in the system is the high-performance infrared detector. Currently, there

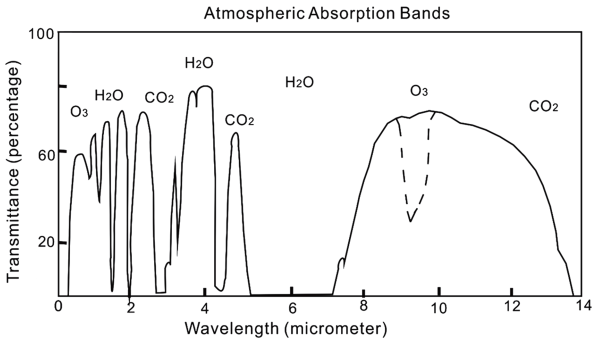


Fig. 1. Transmission spectrum of atmosphere.[1]

*Project supported by the Australian Research Council (Grant Nos. FT130101708, DP170104562, LP170100088, and LE170100233), Universities Australia-DAAD German Research Cooperation Scheme (Grant No. 2014-2015), and a Research Collaboration Award from The University of Western Australia. Facilities used in this work are supported by the WA node of Australian National Fabrication Facility (ANFF).

†Corresponding author. E-mail: wen.lei@uwa.edu.au

© 2019 Chinese Physical Society and IOP Publishing Ltd

are various types of infrared detectors available on the market; however, the high-performance end of infrared imaging market is mainly dominated by HgCdTe infrared detectors due to their unbeatable device performance, such as high quantum efficiency, high responsivity, and fast response rate.

1.2. Current status of HgCdTe infrared detectors

In the past few decades, HgCdTe infrared detectors have developed to be the core technology for the applications in high-performance infrared imaging and sensing. As a ternary alloy semiconductor, the cut-off wavelength of $Hg_{1-x}Cd_xTe$ can be tuned widely to cover the whole infrared region by simply tuning the Cd composition (x value). More importantly, $Hg_{1-x}Cd_xTe$ alloys have high electron mobility and long minority carrier lifetime, resulting in high device performance such as high quantum efficiency ($> 85\%$), high responsivity (the order of $\sim$A/W), and high response rate ($\sim$ns).[2] However, the current state-of-the-art HgCdTe infrared detector technology is based on lattice matched CdZnTe substrates and thus suffers serious limitations including low device yield, high production cost, and small array format size.[3] However, the further development of infrared applications requires the future (next generation) infrared detectors and their focal plane arrays to have new features of lower production cost and larger array format size, which cannot be met with the current HgCdTe infrared detector technology.[3] To address this challenge and achieve HgCdTe infrared detectors with lower cost and larger array format size, significant effort has been devoted to developing alternative substrates to replace CdZnTe substrates for growing high-quality HgCdTe materials. These alternative substrates are required to be of larger wafer size, lower wafer cost, and lower defect density. Over the past several decades, although Si, Ge, and GaAs substrates have been intensively researched as alternative substrates for replacing CdZnTe in order to lower the cost, increase the wafer-size, and increase the array format size, none of them yields HgCdTe with material quality and detector performance comparable to that of HgCdTe grown on CdZnTe due to the high density of dislocations formed in HgCdTe grown on these lattice-mismatched substrates.[3] Most recently, GaSb has also been proposed as a new alternative substrate to replace CdZnTe for growing high-quality HgCdTe materials,[4–7] but significant additional effort is needed before it can be applied in industry.

1.3. HgCdSe infrared materials and detectors

Apart from developing alternative substrates for growing high-quality HgCdTe, another approach to achieve infrared detectors with lower cost and larger array format size is to research new infrared materials which can be lattice-matched grown on substrates with features of larger wafer size and lower wafer cost. Ternary semiconductor alloy HgCdSe provides an ideal candidate for achieving these:[8] (i) tuneable composition and thus cut-off wavelength. The bandgap of $Hg_{1-x}Cd_xSe$, analogues to $Hg_{1-x}Cd_xTe$, can be tuned from 0 to 1.7 eV through adjusting the composition ratio of Hg/Cd; (ii) physical properties favourable for detector application. HgCdSe materials present physical properties similar to HgCdTe, such as electron mobility and minority carrier lifetime, which can lead to infrared detectors with high device performance; (iii) nearly lattice-matched III–V GaSb substrate. Figure 2 shows various semiconductors and their lattice constants.[9] It is observed that HgCdSe alloy is nearly lattice matched to GaSb substrate, which is a high-quality III–V substrate with features of larger wafer size (up to 6 inches in diameter), lower wafer cost, and higher crystal quality (etch pit density as low as $< 10^3$ cm^{-2}).[3,6] Considering that the lattice mismatch between HgCdSe layer and GaSb substrate is only around 0.4%, the ultimate dislocation density in HgCdSe layers grown on GaSb should be below the level of 10^5 cm^{-2}, which will be comparable to that in HgCdTe grown on lattice-matched CdZnTe substrates,[10] and thus be suitable for making high-performance infrared detectors. In the meantime, as shown in Fig. 2, HgCdSe belongs to the family of materials with lattice constants close to 6.1 Å, including ZnTe, GaSb, and InAs, which makes possible the monolithic integration of detector devices capable of sensing different wavelength bands on a single chip. Therefore, HgCdSe materials grown on GaSb substrates in principle provide a feasible solution to the primary challenges faced by current HgCdTe detector technology: high cost and limited array format size. Although some previous work has already been reported on the Bridgman growth of bulk HgCdSe materials and molecular beam epitaxy (MBE) growth of HgCdSe materials on ZnTe/Si substrates, little information is available on HgCdSe materials grown on GaSb substrates. At the University of Western Australia (UWA), we develop the MBE process for growing high-quality HgCdSe on GaSb, and explore its potential application in infrared detectors.[11,12] In this work, we will review our recent research efforts on developing HgCdSe infrared materials on GaSb substrates for making high-performance infrared detectors. At UWA, all HgCdTe samples are grown on GaSb (211)B substrates via MBE technique. In order to achieve high-quality HgCdSe materials, ZnTe buffer layers are grown before growing HgCdSe, and the growth conditions and thickness of the ZnTe buffer layer are optimized to achieve better relaxation of the slight lattice mismatch between HgCdSe and GaSb, and thus minimizing the potential dislocations generated in the epilayers. The growth conditions of HgCdSe are also studied and optimized to achieve HgCdSe epilayers with high material quality, including crystal quality, electrical properties, and optical properties. Our most recent results

indicate that long-wave HgCdSe infrared materials grown on GaSb substrates present electron mobility and minority carrier lifetime comparable to those of the HgCdTe counterpart and can meet the basic material quality requirements for the fabrication of high-performance infrared detectors.

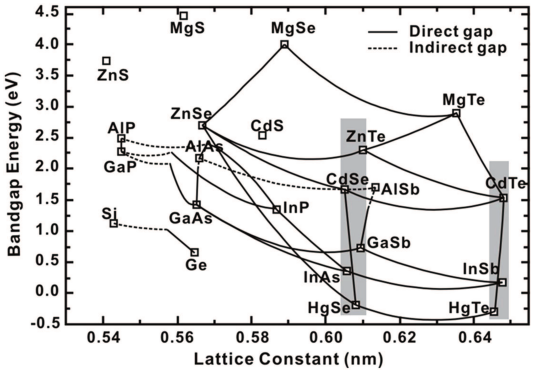


Fig. 2. Energy bandgap of semiconductors vs. lattice constants. Taken from Ref. [9]

2. Experimental details

2.1. Material growth

All of the HgCdSe and ZnTe samples in this work were grown on epi-ready GaSb (211)B substrates in a Riber 32P MBE system. Hg (7N), Cd (6N), Se (5N5), Zn (6N), and Te (6N) were used as the source materials, and standard effusion cells were used to evaporate the source materials without cracking. Note that (211)-orientated GaSb substrates were used due to the fact that Hg atoms have a larger sticking coefficient on the (211)-orientated surface. The epitaxial growth procedure was as follows: following thermal desorption of the native oxide from the GaSb substrate surface at 580 °C for 5 min without Sb background flux protection, the substrate temperature was reduced to 320 °C for growing a ZnTe buffer layer. After that, the substrate temperature was then reduced to the required temperature (70 °C–120 °C) for growing the HgCdSe epitaxial layers. After the growth of HgCdSe, the samples were cooled to room temperature without any background Hg flux. During the growth of ZnTe buffer layers, a typical beam equivalent pressure (BEP) of mid-10^{-7} Torr was used for Zn, while low-10^{-6} Torr was used for Te. During the growth of HgCdSe, a large Hg BEP ($\sim$low–10^{-4} Torr) was used due to the very low sticking coefficient of Hg, while much lower Se BEP ($\sim$low-10^{-6} Torr) and Cd BEP ($\sim$mid-10^{-7} Torr) were used, which are comparable to those used for the MBE growth of HgCdTe.[10] It should be noted that no Sb background flux protection was introduced during the thermal desorption of native oxide from GaSb substrates because Sb is an effective dopant for HgCdSe, and thus can cause contamination to the II–VI MBE growth chamber and unintentional doping to the HgCdSe grown. In order to study the relaxation of lattice mismatch and misfit strain in the materials, the thickness of the ZnTe buffer layer was varied from 150 nm to 1 μm. In order to study the growth mechanism and physical properties of HgCdSe materials, HgCdSe epilayers were grown with different compositions as well as at different substrate temperatures (70 °C–120 °C). The HgCdSe composition was tuned by varying the Se/Cd BEP ratio, which is similar to that reported previously by other research groups.[13,14]

2.2. Material characterization

During the growth of HgCdSe and ZnTe layers, *in-situ* reflection high-energy electron diffraction (RHEED) was applied to undertake real-time monitoring of the surface crystalline quality. The interface structure and composition of the grown HgCdSe and ZnTe samples were characterized with scanning electron microscopy (SEM, Hitachi TM3030) and energy dispersive x-ray spectroscopy (EDX, Hitachi Quantax 70) which was integrated on the Hitachi SEM equipment. The crystal quality was characterized with double crystal x-ray diffraction (XRD) rocking curve measurements (Panalytical Empyrean XRD), while the strain relaxation and dislocation generation in the ZnTe buffer layer were analyzed by XRD reciprocal space mapping (RSM) measurements. The surface morphology and roughness of the HgCdeSe epilayers were measured with atomic force microscopy (AFM, Keysight 5500). The cut-off wavelength of the HgCdSe films was determined by analyzing the transmission spectra measured by Fourier transmission infrared spectroscopy (FTIR, Bruker V70). The alloy composition (x-value) of the $Hg_{1-x}Cd_xSe$ layers was determined through Rutherford backscattering spectrometry (RBS) undertaken by EAG Laboratory. The carrier mobility and carrier concentrations of the HgCdSe epitaxial layers were determined via Hall measurements followed by mobility spectrum analysis (MSA) using a variable magnetic field from 0 to 2 T. Minority carrier lifetimes were measured using the photoconductive decay technique under low-level carrier injection conditions.

3. ZnTe buffer layers and the strain relaxation within

Because ZnTe is nearly lattice-matched to GaSb and HgCdSe, it provides an excellent buffer layer for the subsequent growth of II–VI HgCdSe infrared materials. In addition, the ZnTe buffer layer will also be helpful for electrically isolating HgCdSe from conductive GaSb substrate, as well as preventing possible Ga atom diffusion into HgCdSe.[8] Therefore, the growth of ZnTe buffer layer is essential to the subsequent growth of high-quality HgCdSe epitaxial layer. However, ZnTe is slightly lattice-mismatched with GaSb (0.13%) and thus the thickness of the ZnTe buffer layers must be op-

timized in order to achieve the best relaxation of misfit strain and thus less dislocation generation in the subsequent HgCdSe layers. At UWA, ZnTe buffer layers with different thicknesses (150 nm, 300 nm, 400 nm, 600 nm, and 1000 nm) were grown without growing the subsequent HgCdSe layers, and the lattice mismatch/misfit strain in these samples was analyzed with XRD RSM measurements in order to find the optimum thickness for the ZnTe buffer layer. The RSM measurements were undertaken by doing multiple $\omega/2\theta$ scans with varying ω values. The data of $\omega/2\theta$ scans in real space can be converted into the data in reciprocal space with coordinates q_x and q_y by using the following equations:[15]

$$q_x = \frac{\cos\omega - \cos(2\theta - \omega)}{\lambda}, \quad q_y = \frac{\sin\omega + \sin(2\theta - \omega)}{\lambda},$$

where q_x, q_y, ω, θ, and λ are the Bragg reflection information correlated to profiles along with axes in reciprocal space, incident angle, diffracted angle, and x-ray wavelength, respectively. Note that the RSM measurements were undertaken along with the symmetric (422) direction, which is the crystallographic growth direction of the samples. Figure 3 shows the RSM data taken on the ZnTe buffer layer samples.

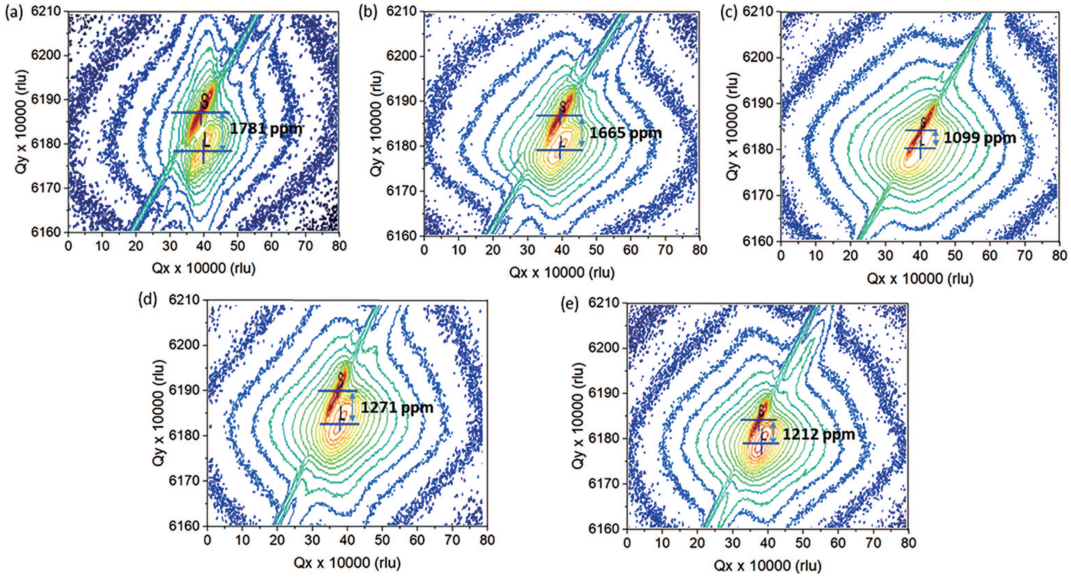


Fig. 3. RSM data for ZnTe buffer layers grown on GaSb substrates with a thickness of (a) 150 nm, (b) 300 nm, (c) 400 nm, (d) 600 nm, and (e) 1000 nm.

For an RSM with a symmetrical scan, the perpendicular mismatch between two diffraction peaks in the RSM indicates the lattice mismatch and strain status. Because the lattice constant of ZnTe (6.105 Å) is larger than that of GaSb (6.095 Å), ZnTe layer grown on GaSb substrate suffers a compressive strain in the plane, but a tensile strain along the growth direction (vertically), which are sketched in Fig. 4. For the MBE growth of ZnTe on GaSb, ZnTe is deposited layer by layer, and the misfit strain caused by the lattice mismatch between ZnTe and GaSb will increase gradually. When the thickness of the ZnTe layer reaches a critical thickness, the strain energy accumulated in the system increases to a level which cannot be accommodated by the material system, and the material system will become unstable. To achieve a stable system, the material system will try to reduce the strain energy by generating misfit defects to relax the misfit strain. This epilayer thickness just before the occurrence of strain relaxation is usually entitled as the critical thickness, which is mainly determined by the lattice mismatch between the two materials in the heterostructures. The smaller the lattice mismatch is, the larger the critical thickness is. To grow high-quality HgCdSe, the thickness of the ZnTe buffer layer must be controlled well below its critical thickness on GaSb.

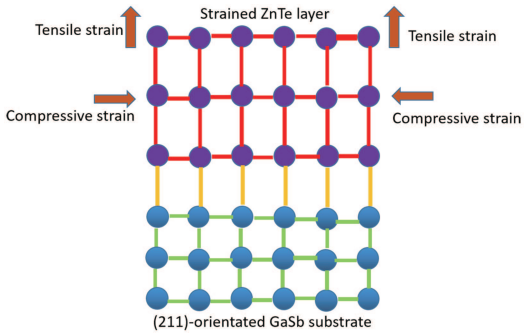


Fig. 4. Schematic diagram of strained ZnTe layer grown on GaSb substrate.

Figure 5 lists the misfit strain along the growth direction measured by the RSM shown in Fig. 3. It can be observed that the misfit strain changes dramatically from the level of 1600 ppm to the level of 1000 ppm when the ZnTe layer thickness increases from 300 nm to 400 nm. This indicates that the strain relaxation occurs once the ZnTe thickness exceeds 300 nm. These results agree well with the calculated critical

thickness (316 nm) of ZnTe layers grown on GaSb(211)B substrate based on the Matthews–Blakeslee model.[16] Hence, to minimize the defect density and obtain high-quality HgCdSe infrared materials, the thickness of the ZnTe buffer layer must be controlled to be below 300 nm. Therefore, a thin ZnTe buffer layer ($\leq$ 200 nm) is used for growing HgCdSe infrared materials in our work.

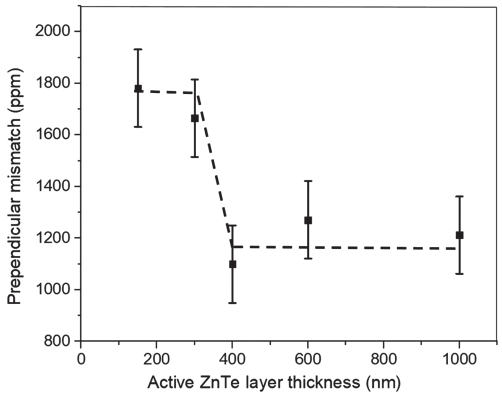


Fig. 5. Misfit strain along the growth direction (vertically) in ZnTe buffer layer samples with different ZnTe layer thicknesses.

4. HgCdSe infrared materials

To understand the growth mechanism and achieve high-quality HgCdSe materials, HgCdSe materials were grown on ZnTe/GaSb with various HgCdSe compositions ($x = 0.18$–0.37) and various HgCdSe thicknesses (3–15 μm) and under various growth temperatures (70 °C–120 °C). Various structural, electrical, and optical characterizations were undertaken to understand the material quality, physical properties, as well as growth mechanism of HgCdSe grown on GaSb substrates.

4.1. Structural characterization

For MBE growth, growth temperature presents significant influence on the material quality of the epitaxial layers, including surface morphology and crystal quality.[9] Figure 6 shows the optical microscope images of the surface of HgCdSe layers grown under growth temperatures ranging from 70 °C to 120 °C while other growth conditions were maintained the same including BEP of the component elements.[12] It is observed that the surface morphology deteriorates with increasing growth temperature. A mirror-like surface is observed for HgCdSe grown under a growth temperature of 70 °C or 80 °C, while surface hillock and/or needle-like defects with regular patterns are observed for HgCdSe grown under a growth temperature over 80 °C. The surface defects observed at higher growth temperatures (> 80 °C) might be caused by the improper BEPs of alloy component elements used for those growth temperatures as the growth temperature can significantly influence the atom sticking coefficient on the surface, especially the Hg atoms. As indicated by the previous work on HgCdTe, these surface defects can seriously degrade the detector performance. Therefore, the growth temperature of HgCdSe needs to be controlled below 80 °C to have a clean, mirror-like surface, which will benefit the yield and performance of infrared detectors made out it.

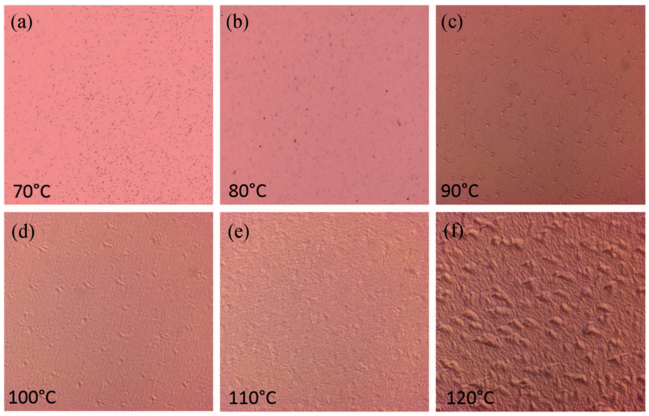


Fig. 6. Microscope images of the surface of HgCdSe epilayers grown under a growth temperature of (a) 70 °C, (b) 80 °C, (c) 90 °C, (d) 100 °C, (e) 110 °C, and (f) 120 °C.[12]

Apart from surface defects, the growth temperature also presents a significant influence on the surface roughness of the HgCdSe epilayers. Figure 7 shows the representative AFM images of the surface of HgCdSe epilayers grown under growth temperatures ranging from 70 °C to 120 °C.[12] It is observed that the surface roughness of the HgCdSe epilayer increases with increasing growth temperature, especially when the growth temperature > 90 °C. This is in agreement with the surface morphology change with increasing growth temperature as shown in Fig. 6. As discussed previously, the surface defects increase with increasing growth temperature, leading to the increased surface roughness observed in Fig. 7. The HgCdSe epilayer grown under a growth temperature of 70 °C presents the smallest surface roughness $\sim$ 2.7 nm. Given that surface morphology is an important measure of the epilayer's crystalline quality, the results in Figs. 6 and 7 suggest that the HgCdSe epilayers grown under a growth temperature of 70 °C should have the best crystalline quality.

Because microscope and AFM imaging can only provide information about the surface quality of the samples, XRD rocking curve measurements were undertaken on HgCdSe epilayers in order to examine the crystal quality of the whole epilayers. Figure 8(a) shows the representative XRD rocking curves of $Hg_{1-x}Cd_xSe$ epilayers grown under a growth temperature of 70 °C, and the XRD full width at half maximum (FWHM) of the HgCdSe samples grown under various growth temperatures, as shown in Figs. 6 and 7. It is observed that the FWHM of the HgCdSe epilayer increases with increasing growth temperature with the smallest FWHM of $\sim$ 116 arcsec for that grown under 70 °C. The monotonically increasing FWHM value of HgCdSe epilayers with increasing growth temperature suggests that the defect density

in the HgCdSe crystals increases with increasing growth temperature, which is well-correlated with the degraded surface morphology of the HgCdSe epilayers with increasing growth temperature. Note that the FWHM of the epi-ready GaSb substrate used in this work is around 37 arcsec, and the FWHM of 116 arcsec for HgCdSe grown under 70 °C indicates a high crystalline quality. In addition to surface defects, threading dislocations in the materials also seriously affect the yield and performance of detectors, which presents another important material parameter needed to be studied. As currently there is no standard etchant for revealing the dislocations in HgCdSe, at UWA the etch pit density (EPD) measurements of HgCdSe were undertaken by using a 30 s etch for revealing dislocations in CdSe substrates.[11] As shown in Fig. 8(b), circular pits of 10–20 μm in size with a density of $\sim 2.2 \times 10^3$ cm^{-2} are observed on the surface of the HgCdSe epitaxial layers.[11] This etch pit density is three orders of magnitude lower than that of HgCdSe materials grown on ZnTe/Si substrates (1×10^6–6×10^6 cm^{-2}) reported previously,[17] and comparable to that of the GaSb substrate (∼low-10^3 cm^{-2}). Such a low etch pit density is mainly due to the nearly lattice-matched growth of HgCdSe and ZnTe on GaSb, in comparison to the large-lattice-mismatched growth of HgCdSe and ZnTe on Si reported previously.[17] This low etch pit density suggests the high crystal quality of HgCdSe epitaxial layers grown at UWA.

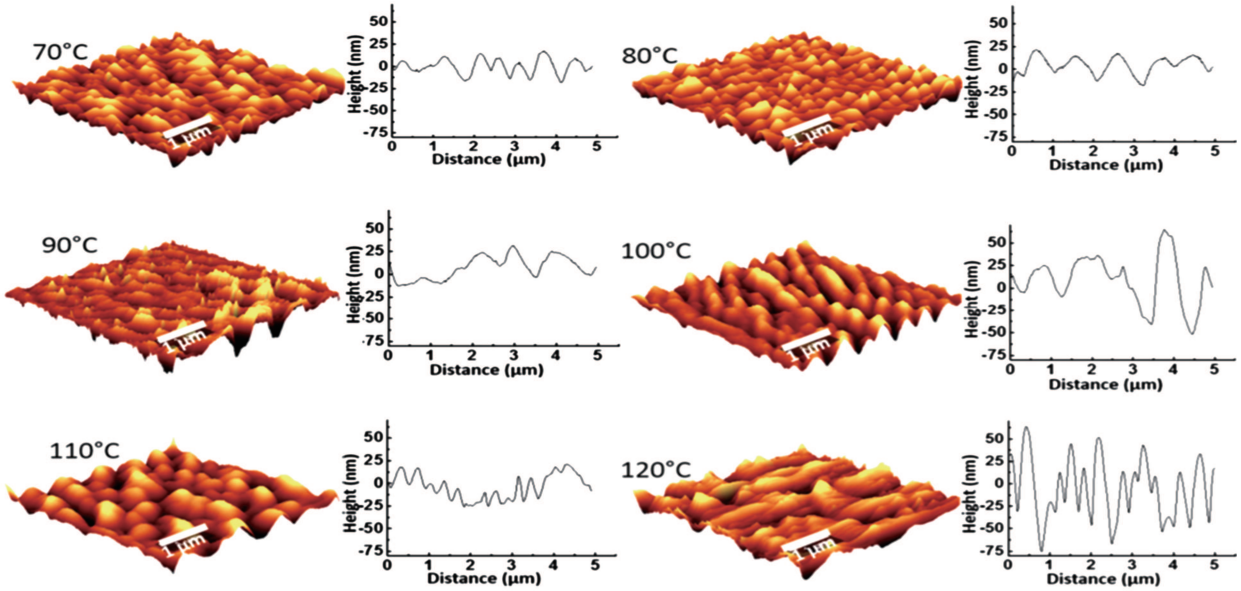


Fig. 7. Three-dimensional AFM images and lateral height profiles of HgCdSe epilayers grown under growth temperatures ranging from 70 °C to 120 °C.[12]

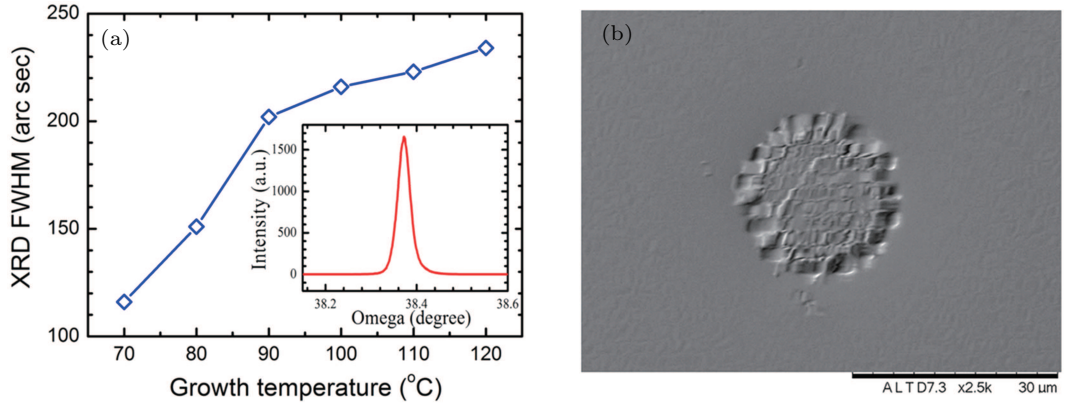


Fig. 8. (a) XRD FWHM of HgCdSe epilayers grown under various growth temperatures ranging from 70 °C to 120 °C; (b) representative SEM images of the HgCdSe surface after the 30 s EPD etch.[11] Inset of (a) shows the representative XRD rocking curve for HgCdSe grown under a growth temperature of 70 °C.

4.2. Optical characterization

Apart from structural characterization, at UWA significant effort has been devoted to studying the optical properties of HgCdSe epilayers, mainly the cut-off wavelength of HgCdSe with various alloy compositions and under various temperatures. Figure 9(a) shows the FTIR transmission spectra of HgCdSe samples grown with different Se/Cd BEP ratios, which were measured at a temperature of 80 K.[11] It is observed that with increasing the Se/Cd BEP ratio from 6 to

7.8, the corresponding cut-off wavelength of the $Hg_{1-x}Cd_xSe$ epilayer varies from 3.9 μm to 10.4 μm. This change of cut-off wavelength with varying the Se/Cd BEP ratio is caused by the corresponding change of the HgCdSe alloy composition. With RBS measurements undertaken at EVG, the x-value of the $Hg_{1-x}Cd_xSe$ alloy is determined to be 0.18, 0.19, 0.21, and 0.37 for HgCdSe with a cut-off wavelength of 10.4 μm, 9 μm, 6.6 μm, and 3.9 μm, respectively. Such tuneable-wavelength capability of HgCdSe is very similar to that of HgCdTe, where the cut-off wavelength/composition can also be tuned by varying the Te/CdTe BEP ratio.[18]

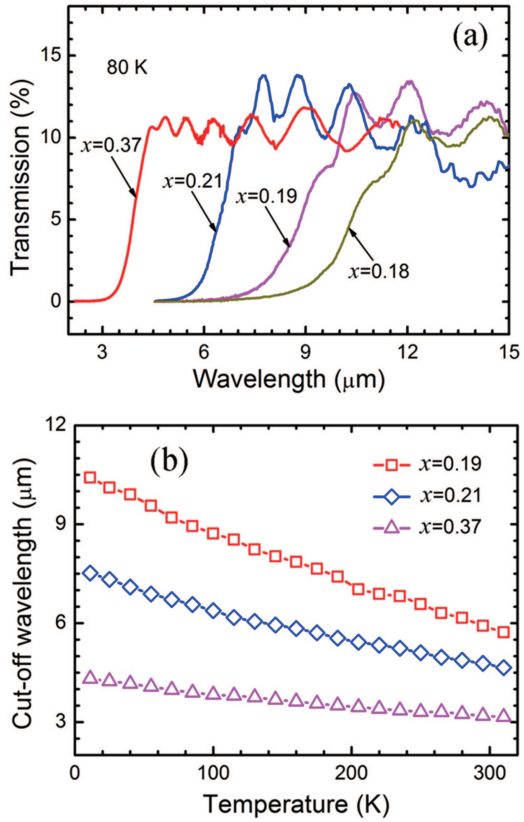


Fig. 9. (a) FTIR transmission spectra of $Hg_{1-x}Cd_xSe$ samples with x values of 0.18, 0.19, 0.21, and 0.37 measured at 80 K; (b) temperature dependent cut-off wavelengths of $Hg_{1-x}Cd_xSe$ samples with x values of 0.19, 0.21, and 0.37.

To further explore the bandgap behavior of $Hg_xCd_{1-x}Se$, temperature-dependent FTIR measurements were also carried out on the $Hg_{1-x}Cd_xSe$ samples with x values of 0.37, 0.21, and 0.19. Figure 9(b) shows the cut-off wavelength measured at different temperatures for HgCdSe with x values of 0.37, 0.21, and 0.19.[11] Obviously, the cut-off wavelength presents a consistent blue-shift with increasing temperature, which is very similar to the behavior of HgCdTe.[19] Similar to HgCdTe alloy, such a blue shift of cut-off wavelength with increasing temperature is mainly caused by the electron–phonon interaction (mainly acoustic phonons) in the alloy material.[20] As noted in Fig. 9(b), the observed blue shift of the cut-off wavelength with increasing temperature is much greater for low x-value alloys, that is, for alloys with a higher HgSe/CdSe ratio,[21] which is also similar to the case of HgCdTe alloy. These FTIR studies suggest that the HgCdSe material shows a bandgap behavior similar to HgCdTe, and thus the whole range of infrared band can be covered by varying the alloy composition of HgCdSe.

4.3. Electrical characterization

For infrared detector applications, the two main physical parameters which directly impact on the device performance of infrared detectors are the carrier's mobility and the minority carrier lifetime of the infrared materials. Because GaSb substrates are conductive, standard Hall analysis cannot separate the Hall signal of HgCdSe layers from that of GaSb. At UWA, in order to determine the carrier mobility in HgCdSe, MSA measurements were undertaken on the HgCdSe samples, which allow the conductivity contribution of the HgCdSe epitaxial layer to be separated from that of the conductive GaSb substrate.[22] Note for this MSA measurement, standard Van der Pauw Hall measurements were first performed on HgCdSe materials, and then MSA technique was used to fit the raw Hall data to identify the conductivity contribution of $Hg_{1-x}Cd_xSe$ sample and that of GaSb substrate.[22] Figure 10 shows the representative MSA spectra of a GaSb substrate and an as-grown HgCdSe sample ($x = 0.18$, 10.4 μm cut-off wavelength at 80 K) measured at 132 K, respectively. Obviously, the carrier signal of the GaSb substrate has been successfully separated from that of HgCdSe by using MSA technique. It is observed that the as-grown HgCdSe shows typical n-type behavior with an electron concentration of around 1.9×10^{16} cm^{-3}, and an electron mobility of around 6.8×10^4 $cm^2 \cdot V^{-1} \cdot s^{-1}$. The n-type behavior can be attributed to the existence of native Se vacancies and other impurities, as discussed in previous work.[14]

To better understand the electrical properties of HgCdSe, temperature dependent MSA measurements were also undertaken on the HgCdSe sample with $x = 0.18$. Figure 11 presents the electron mobility and background electron concentration of HgCdSe with $x = 0.18$ measured at different temperatures.[11] Obviously, the electron mobility increases with reducing temperature, however, the background electron concentration decreases with reducing temperature. At 80 K, the electron mobility of the dominant carrier is measured to be 1.3×10^5 $cm^2 \cdot V^{-1} \cdot s^{-1}$ and the background electron concentration to be 1.6×10^{16} cm^{-3}. This electron mobility is significantly higher than that reported for the counterpart LWIR HgCdSe in previous work, which was in the range of 2.5×10^4–3×10^4 $cm^2 \cdot V^{-1} \cdot s^{-1}$,[14] and is comparable to that ($\sim 1.5 \times 10^5$ $cm^2 \cdot V^{-1} \cdot s^{-1}$) of counterpart LWIR $Hg_{1-x}Cd_xTe$ ($x = 0.22$, ~ 10.7 μm cut-off wavelength at 80 K) grown on lattice-matched CdZnTe substrates.[23,24] This indi-

cates the high crystal quality of the HgCdSe epitaxial layers grown, which agrees with the structural characterization of the HgCdSe epilayer discussed in the previous sections.

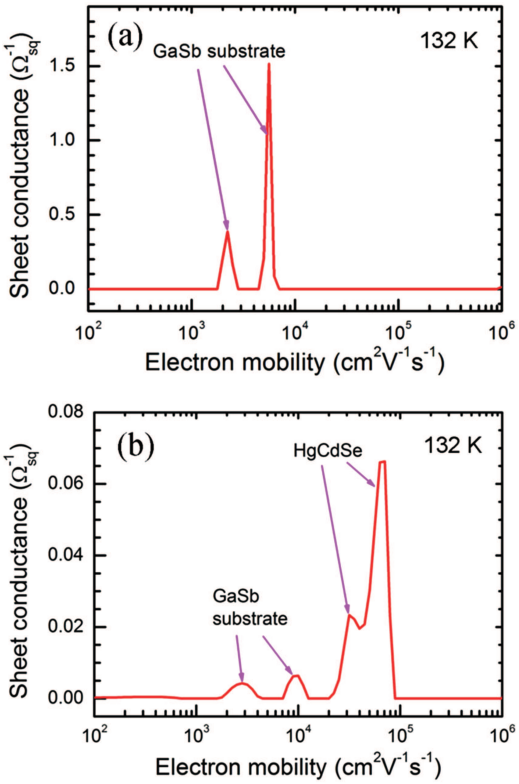


Fig. 10. Electron mobility spectrum at 132 K of (a) GaSb substrate only and (b) HgCdSe ($x = 0.18$) epilayer grown at 70 °C on GaSb substrate.[11]

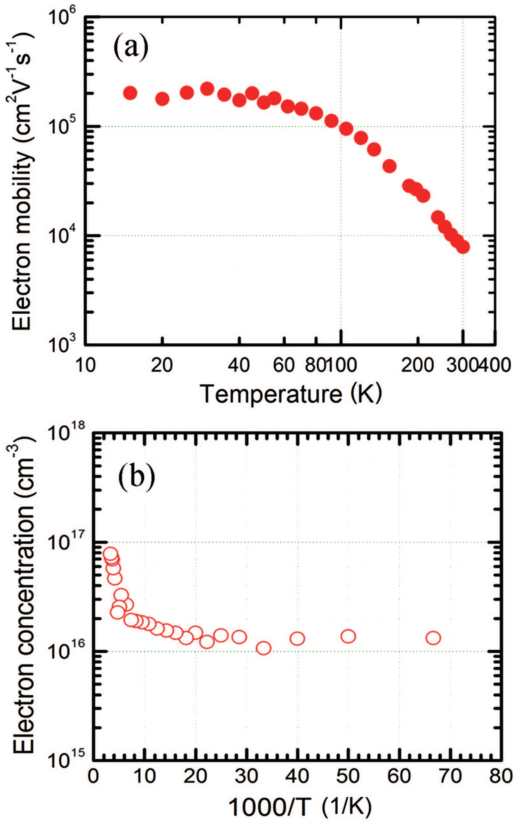


Fig. 11. Temperature dependent (a) electron mobility and (b) electron concentration of as-grown HgCdSe ($x = 0.18$) grown at 70 °C on GaSb substrate.[11]

Apart from carrier mobility, minority carrier lifetime is another important physical parameter impacting the performance of infrared detectors. At UWA, photoconductive decay measurements were used to study the minority carrier lifetime in the HgCdSe epitaxial layers grown on GaSb. Figure 12(a) presents the photoconductive decay curve of an as-grown HgCdSe sample with $x = 0.18$ measured at 80 K.[11] To determine the minority carrier lifetime, the raw decay curve data was fitted with the following exponential equation:[25]

$$y = y_0 + A_1 e^{-x/\tau}, \tag{1}$$

where y_0 and A_1 are the fitting parameters, and τ is the minority carrier lifetime to be fitted. The minority carrier lifetime is determined to be 2.22 μs for the LWIR HgCdSe ($x = 0.18$) material. Such a minority carrier lifetime of 2.22 μs is significantly longer than that (∼ 132 ns) reported for the counterpart HgCdSe in previous work,[26] and is comparable to that (∼ 2 μs) of the counterpart LWIR $Hg_{1-x}Cd_xTe$ ($x = 0.22$, ∼ 10.7 μm cut-off wavelength at 80 K) materials grown on lattice-matched CdZnTe substrates.[24,27] This further indicates the high crystal quality of our HgCdSe materials grown on GaSb. Figure 12(b) shows the minority carrier lifetime of HgCdSe ($x = 0.18$) measured at various temperatures ranging from 80 K to 300 K. Obviously, a > 2 μs minority carrier lifetime can be maintained approximately up to 175 K. This suggests that HgCdSe materials could be used for fabricating infrared detectors that can operate at higher temperatures in comparison to the current HgCdTe infrared detectors (mainly operating at temperatures < 100 K).[3]

As discussed in Subsection 4.1, the growth temperature presents a significant influence on the structural properties of HgCdSe. Similarly, the growth temperature can also have a significant influence on the electrical properties of HgCdSe. To study the impact of growth temperature on electrical properties, MSA and photocurrent decay measurements were also undertaken on HgCdSe samples with similar x values (∼ 0.18) but grown at different growth temperatures ranging from 70 °C to 120 °C. Table 1 shows the XRD FWHM, electron mobility, and minority carrier lifetime measured for the HgCdSe materials grown at 70 °C, 80 °C, 100 °C, and 120 °C.[11] Obviously, the growth temperature has a significant impact on the material quality, and lower growth temperature leads to higher material quality: narrower XRD FWHM, higher electron mobility, and longer minority carrier lifetime. As shown in Table 1, the growth temperature of 70 °C gives the best material quality for HgCdSe in our UWA MBE facility. This is well correlated with the influence of the growth temperature on the structural properties of HgCdSe as shown in Figs. 6 and 7. Similar to the higher structural quality when grown at lower growth temperatures, the main reason for the better

material quality of HgCdSe when grown at lower growth temperatures is the fact that Hg atoms have very a low sticking coefficient at higher temperatures.[7] and thus the lower growth temperatures are required to ensure that there are adequate Hg atoms on the material growth front for growing single crystal material, resulting in higher crystal quality at lower growth temperature.[11] Note that this could also be the main reason for the material quality difference between the HgCdSe materials grown at UWA and those reported previously, which were grown at higher temperature ~ 100 °C.[9] Apart from the lower growth temperature, the nearly lattice-matched growth of ZnTe and HgCdSe on GaSb could contribute to the higher material quality of HgCdSe grown at UWA due to the lower dislocation density formed in the materials, in comparison to the lattice-mismatched growth of ZnTe and HgCdSe on Si, as reported previously.[17]

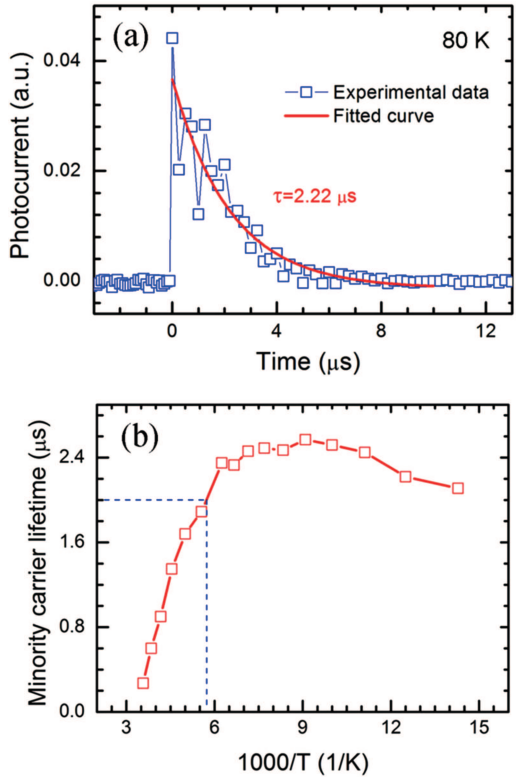


Fig. 12. (a) The 80 K photoconductive decay measurement and (b) temperature dependent minority carrier lifetime of HgCdSe ($x = 0.18$) grown at 70 °C on GaSb substrate.[11]

Table 1. XRD FWHM, electron mobility, and minority carrier lifetime of HgCdSe ($x = 0.18$) materials grown at different growth temperatures.[11]

Growth temperature/°C	70	80	100	120
XRD FWHM/arcsec	116	151	216	234
Electron mobility@132 K/10^4 cm^2/V·s	6.8	2.0	2.2	1.5
Minority carrier lifetime@80 K/μs	2.2	1.35	1.1	0.71

5. Conclusions and future work

In this work, we have reviewed our recent efforts on developing HgCdSe infrared materials on GaSb substrates for fabricating infrared detectors with new features of lower cost and larger array format size. At UWA, HgCdSe materials are grown via MBE on ZnTe/GaSb substrates, instead of ZnTe/Si substrates in order to leverage the benefit of nearly lattice-matched growth of ZnTe and HgCdSe on GaSb. The study on the strain/lattice mismatch relaxation in ZnTe buffer layers grown on GaSb shows that the thickness of the ZnTe buffer layer needs to be controlled below 300 nm in order to minimize the generation of misfit dislocations in the material system and thus achieve high-quality HgCdSe grown subsequently. The cut-off wavelength/alloy composition of HgCdSe materials can be tuned widely from SWIR, to MWIR, and to LWIR by varying the Se/Cd BEP ratio during the HgCdSe growth. Growth temperature presents significant impact on the material quality of HgCdSe materials including surface defects, surface roughness, and electrical properties, and lower growth temperature can lead to higher material quality for HgCdSe materials. With the optimizing growth temperature, HgCdSe materials grown at UWA present high material quality with electron mobility and minority carrier lifetime that are significantly improved over the values obtained in previous work, and comparable to those for counterpart HgCdTe materials grown on lattice-matched CdZnTe substrates. Typically, LWIR HgCdSe ($x = 0.18$, 80 K cut-off wavelength of 10.4 μm) presents an electron mobility of 1.3×10^5 cm^2·V^{-1}·s^{-1} with a background electron concentration of 1.6×10^{16} cm^{-3} at 80 K, and a minority carrier lifetime of 2.2 μs at 80 K. This indicates that HgCdSe grown at UWA. In particular, LWIR can meet the basic material quality requirements to make high-performance infrared detectors.

Although significant progress has been made in developing HgCdSe infrared materials on GaSb substrates, it is still quite challenging to achieve their ultimate industry applications. One of the main challenges is the high level of background electron concentration in as-grown HgCdSe materials. Despite the fact that the background electron concentration in our as-grown HgCdSe epitaxial layers, e.g., 1.6×10^{16} cm^{-3} for LWIR HgCdSe ($x = 0.18$, 80 K) is one order of magnitude lower than the corresponding value reported in previous studies,[26] this level of background electron concentration, however, is not suitable for making high performance advanced infrared detectors based on p–n junctions. The background carrier concentration needs to be controlled below the low-10^{15} cm^{-3} level to allow effective and controllable extrinsic doping in the 10^{16} cm^{-3} range or above, which is required for fabricating p–n junctions for high-performance detectors based on photovoltaic and/or other modern device structures. Therefore, it is essential to reduce the background carrier concentration in HgCdSe materials. There are several potential approaches to address this challenge: (i) post-growth thermal annealing in a Se environment. As the high level

of background carrier concentration in the as-grown HgCdSe is mainly caused by Se vacancies in HgCdSe material, post-growth thermal annealing in a Se environment can significantly reduce the Se vacancies, and thus effectively reduce the background doping concentration. One order of magnitude reduction in background electron concentration has been demonstrated for HgCdSe after post-growth annealing in a Se environment.[8] With further optimizing the annealing process, the background electron concentration can be further reduced. (ii) Utilization of higher purity Se source material for growing HgCdSe. At UWA, only 5N5 purity Se source material is used for growing HgCdSe materials. It has been demonstrated that higher purity Se source material can also effectively reduce the level of impurities in the HgCdSe epilayer, and thus the background doping concentration.[8] If Se source material with 7N purity or above is commercially available, it can be expected that the background electron concentration can be significantly reduced. (iii) Guttering/filtering of Se vacancies and impurities. It has been demonstrated in HgCdTe material that defects and impurities can be significantly reduced with properly designed gettering/filtering structures,[3] which can also be applied to HgCdSe materials. Therefore, it can be expected that a background electron concentration level within the low-10^{15} cm^{-3} range or even lower is achievable for HgCdSe with implementing the above approaches.

In summary, the MBE growth of HgCdSe on GaSb substrates is only a recent effort, and even higher quality HgCdSe materials are expected with further effort on this. Although significant amount of work is required to control the background electron concentration to $<$ low-10^{15} cm^{-3}, the preliminary results achieved at UWA are highly encouraging and clearly show the great potential of HgCdSe materials for fabricating next generation infrared detectors with features of lower cost and larger array format size.

References

[1] Butler M J A, Mouchot M C, Barale V and LeBlanc C 1988 *FAO Fish. Tech. Pap.* **295** 165

[2] Norton P 2002 *Optoelectronics Rev.* **3** 159

[3] Lei W, Antoszewski J and Faraone L 2015 *Appl. Phys. Rev.* **2** 041303

[4] Lei W, Gu R, Antoszewski J, Dell J and Faraone L 2014 *J. Electron. Mater.* **43** 2788

[5] Lei W, Ren Y, Madni I and Faraone L 2018 *Infrared Phys. Techn* **92** 96

[6] Lei W 2018 *J. Nanoscience Nanotechnol.* **18** 7349

[7] Lei W, Gu R, Antoszewski J, Dell J, Neusser G, Sieger M, Mizaikoff B and Faraone L 2015 *J. Electron. Mater.* **44** 3180

[8] Doyle K 2013 *Development of HgCdSe for Third Generation Focal Plane Arrays using Molecular Beam Epitaxy* (Ph. D. Thesis) (West Virginia University)

[9] Brill G, Chen Y and Wijewarnasuriya P 2011 *J. Electron. Mater.* **40** 1679

[10] Reddy M, Peterson J, Lofgreen D, Vang T, Patten E, Radford W and Johnson S 2010 *J. Electron. Mater.* **39** 974

[11] Lei W, Ren Y, Madni I, Umana-Membreno G and Faraone L 2018 *Infrared Phys. Tech.* **92** 197

[12] Madni I, Membreno G, Lei W and Faraone L 2018 *J. Electron. Mater.* **47** 5691

[13] Brill G N, Chen Y, Wijewarnasuriya P S and Dhar N K 2012 *Phys. Status Solidi (a)* **209** 1423

[14] Doyle K, Swartz C H, Dinan J H, Myers T H, Brill G, Chen Y, VanMil B L and Wijewarnasuriya P 2013 *J. Vac. Sci. Technol. B* **31** 03C124

[15] Capper P, Harris J E, O'Keefe E S, Jones C L and Gale I 1995 *Advanced Mater. For Opt. Electron.* **5** 101

[16] Chai J, Noriega O C, Dinan J H and Myers T H 2012 *J. Electron. Mater.* **41** 3001

[17] Brill G and Chen Y P 2011 *Development of 6.1 Å materials for IR applications*, Project report (ARL-TR-5855), Army Research Lab, US

[18] Wenisch J, Schirmacher W, Wollrab R, Eich D, Hanna S, Breiter R, Lutz H and Figgemeier H 2015 *J. Electron. Mater.* **44** 3002

[19] Garl, J and Capper P 2011 *Mercury Cadmium Telluride: Growth, Properties and Applications* (West Susses: John Wiley) Chap. **12** pp. 275–295

[20] Krishnamurthy S, Chen A B , Sher A and Van Schilfgaarde M 1995 *J. Electron. Mater.* **24** 1121

[21] Guenzer C S and Bienenstock A 1973 *Phys. Rev. B* **8** 4655

[22] Chandrasekhar Rao T, Antoszewski J, Faraone L, Rodriguez J, Plis E and Krishna S 2008 *Appl. Phys. Lett.* **92** 012121

[23] Carmody M, Edwall D, Ellsworth J, Arias J, Groenert M, Jacobs R, Almeida L, Dinan J, Chen Y and Brill G 2007 *J. Electron. Mater.* **36** 1098

[24] Swartz C, Tompkins R, Giles N, Myers T, Edwall D, Ellsworth J, Piquette E, Arias J, Berding M and Krishnamurthy S 2004 *J. Electron. Mater.* **33** 728

[25] Cui H, Zeng J, Tang N and Tang Z 2013 *Opt. Quant Electron.* **45** 629

[26] Doyle K, Swartz C, Pattison J, Chen Y and Myers T 2013 *Electron Transport and Minority Carrier Lifetime in HgCdSe, in: 2013 II-VI Workshop,* Chicago, Illinois, October 1-3, 2013

[27] Kinch M, Brau M and Simmons A 1973 *J. Appl. Phys.* **44** 1649